International Journal of Pharmaceutics: X 7 (2024) 100235

Contents lists available at ScienceDirect

International Journal of Pharmaceutics: X

journal homepage: www.sciencedirect.com/journal/international-journal-of-pharmaceutics-x

Dual-responsive chondroitin sulfate self-assembling nanoparticles for combination therapy in metastatic cancer cells

Ensieh Poursani [a,1], Giuseppe Cirillo [b,1], Manuela Curcio [b,*], Orazio Vittorio [c], Michele De Luca [b], Antonella Leggio [b], Fiore Pasquale Nicoletta [b], Francesca Iemma [b]

[a] Children's Cancer Institute, Lowy Cancer Research Centre, University of New South Wales, Randwick, NSW 2052, Australia
[b] Department of Pharmacy Health and Nutritional Science, University of Calabria, Rende 87036, Italy
[c] School of Biomedical Science, University of New South Wales, Randwick, NSW 2052, Australia

ARTICLE INFO

Keywords:
Stimuli-responsive release
Prodrugs
Self-assembling nanoparticles
Co-delivery

ABSTRACT

In this study, we developed self-assembling nanoparticles (LCPs) able to trigger the release of Chlorambucil (Chl) and Doxorubicin (DOX) to MDA-MB-231 cells by exploiting the enzyme and redox signals. The DOX loaded LCPs was prepared by the self-assembly of two chondroitin sulphate (CS) derivatives, obtained by the covalent conjugation of Lipoic Acid (LA) and Chlorambucil (Chl) to the CS backbone. After the physic-chemical characterization of the conjugates by FT-IR, ^{1}H NMR, and determination of the critical aggregation concentration, spherical nanoparticles with mean hydrodynamic diameter of 45 nm (P.D.I. 0.24) and *Z*-potential of - 44 mV were obtained by water addition/solvent evaporation method. In vitro experiments for the release of Chl and DOX were performed in healthy and cancer cells, using a cell culture media to maintain the physiological intracellular conditions (pH 7.4) (and concentration of esterase and GSH. The results allowed the selective release of the payloads to be detected: Chl release of 0 and 41% were obtained after 2 h incubation in normal and in cancer cells respectively, while values of 35 (in healthy cells) and 60% (in cancer cells) were recorded for DOX release after 96 h. Finally, viability studies proved the ability of the newly proposed nanosystem to enhance the cytotoxic activity of the two drugs against cancer cells.

1. Introduction

Stimuli-responsive nanoparticles are a promising class of drug delivery systems with unique bio-responsive physicochemical properties (Kaushik et al., 2022; Li et al., 2020). These "smart" carriers can respond in a predictable and specific way to exogenous or endogenous stimuli from the pathological site by changing their structure, solubility, surface properties, shape or self-association/dissociation behaviors, thus improving the cellular uptake and the endosomal escape and triggering the intracellular release of a loaded drug (Karimi et al., 2016; Wang et al., 2022). When applied to cancer therapy, stimuli-responsive nanocarriers gain particular interest by virtue of the characteristic differences between tumour and normal tissues (Huda et al., 2020; Zhou et al., 2022). Tumour microenvironment is indeed characterized by alterations of pH, redox state, and reactive oxygen species production, as well as by hypoxia and enzymes overexpression (Baghba et al., 2020; Dzobo et al., 2023). All these metabolic abnormalities are potential internal stimuli to be exploited for the design of stimuli-responsive materials (He et al., 2020; Li and Burgess, 2020).

In particular, glutathione (GSH), the most abundant reductant involved in cells detoxification and antioxidant mechanisms, presents blood and extracellular matrix concentrations (~20 μM) significantly lower than that recorded in the intracellular space (~10 mM), a value further enhanced (~10-folds) in the tumour tissues (Quinn et al., 2017; Zhang et al., 2018). Furthermore, compared to non-malignant cells, tumour tissues showed altered activity and expression of important enzymes, such as matrix metalloproteinases, hyaluronidases, and esterase (Dong et al., 2019; Qiu et al., 2018). Thus, materials able to precisely release their payload in the pathological site can be achieved by endowing the nanoparticles with GSH and/or enzyme-responsive functional groups, with a notable improvement of the drug efficacy and a reduction of the insurgence of multidrug resistance (MDR) phenomena (Yi et al., 2023). Typically, the redox responsivity can be obtained by introducing reducible disulfide, diselenide, and succinimide-

* Corresponding author at: Department of Pharmacy Health and Nutritional Science, University of Calabria, Rende 87036, Italy.
E-mail address: manuela.curcio@unical.it (M. Curcio).
[1] these authors equally contributed

https://doi.org/10.1016/j.ijpx.2024.100235
Received 23 May 2023; Received in revised form 19 January 2024; Accepted 28 February 2024
Available online 5 March 2024

thioether linkages (Guo et al., 2018), while esters, peptides and glycosidic bonds are key examples of chemical specimens cleavable by overexpressed enzymes (Liang et al., 2021; Shahriari et al., 2019).

In recent years, natural polymers, and polysaccharides in particular, have gained much attention as base materials for the preparation of nanoparticulate systems, because of their biocompatibility and chemical versatility, allowing the obtainment of a plethora of drug delivery systems with a variety of architectures and applications (Barclay et al., 2019; Brindisi et al., 2022; Khalid et al., 2021; Liu et al., 2022). Among others, the anionic glycosaminoglycan chondroitin sulfate (CS) has emerged as an interesting material because of its high selectivity for CD44 receptors and the presence of many functional groups suitable for chemical derivatization with biological molecules (Luo et al., 2019; Shi et al., 2021; Yu et al., 2023).

In this work, a stimuli-responsive nanosystem for the co-delivery of two anticancer drug, Chlorambucil (Chl) and Doxorubicin (DOX), was designed and tested in triple negative breast cancer cells. More in details, two distinct CS conjugates, CS-Chl and CS-LA, were synthesized by covalent insertion of the anticancer drug Chlorambucil (Chl) and the antioxidant molecule lipoic acid (LA) on the polysaccharide backbone, respectively. The CS-Chl conjugate could work as an esterase-responsive prodrug, while CS-LA conjugate was designed to possess a GSH-response activity due to the presence of disulfide bonds in the LA pendant groups. Besides the functional properties, the insertion of both LA and Chl hydrophobic moieties is expected to confer amphiphilic characteristics to the final conjugates, which were eventually combined to obtain self-assembling nanoparticles (LCPs) able to simultaneously vectorize the conjugated Chl and the loaded DOX (Fig. 1). To the best of our knowledge, this is the first example of polysaccharide self-assembling nanoparticles coupling, within the same formulation, the advantages of *co*-delivery and polymeric prodrugs approaches with the stimuli-responsive strategy.

The proposed nanoparticles were characterized in terms of size, shape, surface charge and in vitro esterase-GSH triggered release of Chl and DOX, respectively. Then, biological characterization allowed the effectiveness of nanoformulation as intracellular delivery vehicle for the cytotoxic drugs to be elucidated.

2. Materials and methods

2.1. Synthesis of CS-LA conjugate

CS (0.2 g, 0.5 mmol disaccharide repeating units) was dissolved in 5 mL distilled H_2O. Then, N-ethylcarbodiimide hydrochloride (EDC) (0.037 g, 0.19 mmol), N-hydroxysuccinimide (NHS) (0.021 g, 0.19 mmol) and lipoic acid (LA) (0.02 g, 0.097 mmol), previously dissolved in 5 mL DMSO, were added to the CS solution. The mixture was magnetically stirred for 24 h at 25 °C. The product CS-LA was isolated by dialysis (MWCO 12–14 kDa) against DMSO/H_2O (1:1 *v*/v) for 48 h and against distilled H_2O for 24 h, and then freeze dried (Yield: 92%). ^{1}H NMR measurements (Bruker Avance 300, Bruker Italy, Milan, Italy, 25 °C, DMSO-d_6/D_2O 1:1 v/v,) and FT-IR spectra (Jasco FT-IR 4200, Easton, MD, USA) were performed to qualitatively characterize the conjugate, while the amount of LA covalently attached to CS was determined by Ellman's assay by preliminary reducing the disulfide bonds of LA moieties with GSH (CS-LA_{red}) (Curcio et al., 2015a). Briefly, 20 mg CS-LA conjugate were dissolved in 3 mL GSH water solution (50 mM) at 37 °C for 1 h under magnetic stirring, the solution was dialyzed (MWCO 12–14 kDa) against distilled H_2O for 24 h to remove GSH, and the CS-LA_{red} recovered by freeze-drying. Aliquots (250 μL) of CS-LA_{red} (5 mg mL^{-1}) were mixed with 0.5 M NaH_2PO_4/Na_2HPO_4 phosphate buffer pH 8.0 (250 μL) and Ellman's reagent (500 μL; 0.3 mg mL^{-1} of 5,5′-dithiobis-2-nitrobenzoic acid (DTNB) in 0.05 M NaH_2PO_4/Na_2HPO_4 phosphate buffer pH 8.0). The reaction was allowed to proceed for 2 h at

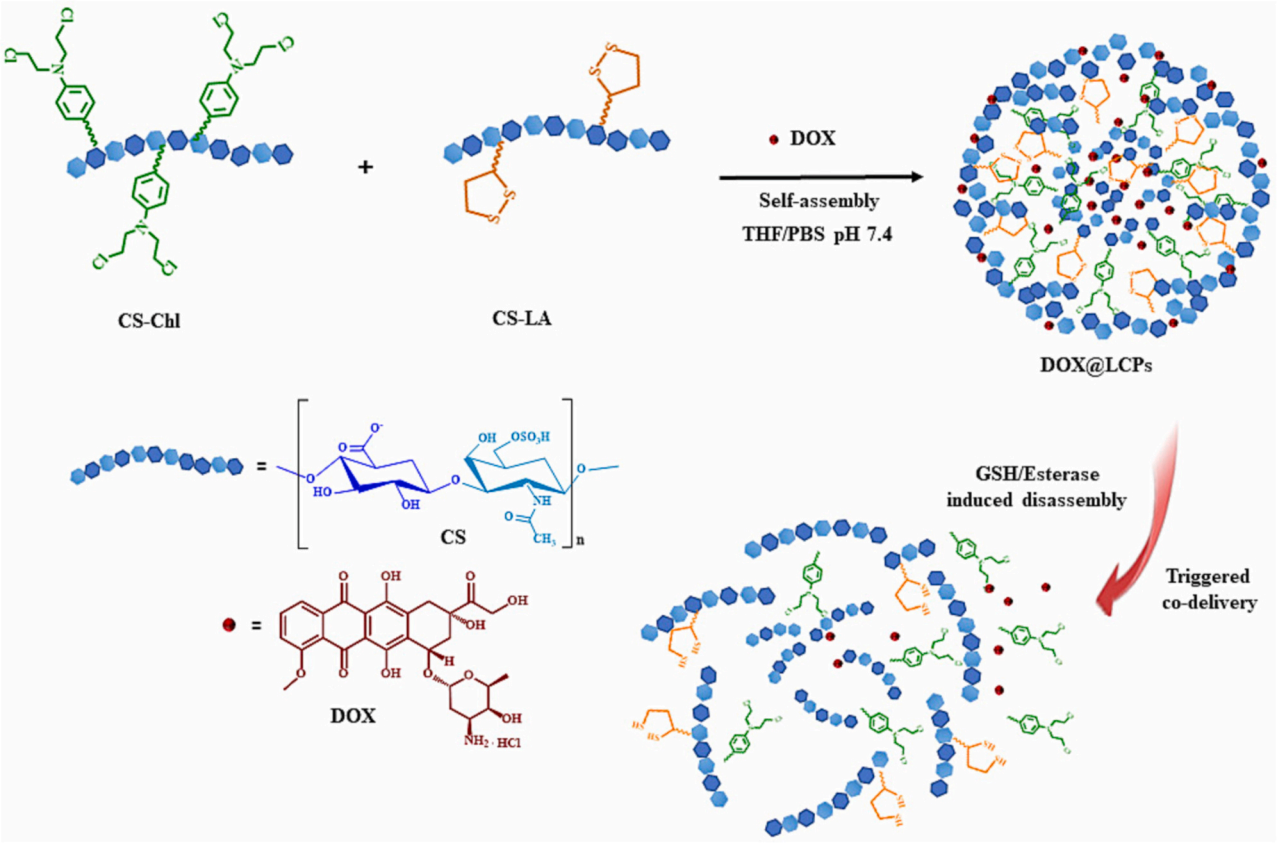

Fig. 1. Representation of the DOX-loaded nanoparticle formation and triggered destabilization/codelivery in intracellular-mimicking conditions.

room temperature and the absorbance was measured at 420 nm. CS-LA was used as control and processed under the same conditions. The amount of thiol moieties was calculated from a calibration curve elaborated from solutions of cysteine (0.05 to 0.45 mM) and expressed as millimoles of free sulfhydryl groups per gram of CS-LA.

FITC-labeled CS-LA conjugate was prepared by mixing 60 mg of CS-LA dissolved in 3 mL of $NaHCO_3$ solution (pH 8.5) with 2 mL of FITC solution (2.4 mg mL^{-1}). The mixture was incubated at r.t. for 12 h, then the FITC-labeled CS-LA (FITC-CS-LA) was dialyzed against distilled water for 72 h and freeze dried.

All chemicals were purchased from Merck/Sigma Aldrich, Germany.

2.2. Synthesis of CS-Chl conjugate

CS (0.2 g, 0.5 mmol disaccharide repeating units) was dissolved in 5 mL distilled H_2O. Then, 8 mL DMSO solution of N-ethylcarbodiimide hydrochloride (EDC) (0.115 g, 0.6 mmol), N-hydroxysuccinimide (NHS) (0.069 g, 0.6 mmol) and Chlorambucil (Chl) (0.121 g, 0.40 mmol) were added to the CS solution. The mixture was magnetically stirred for 24 h at room temperature. The product CS-LA was isolated by dialysis (MWCO 12–14 kDa) against DMSO/H_2O (1:1 *v*/v) for 48 h and against distilled H_2O for 24 h, then freeze dried (Yield: 92%). ^1H NMR measurements (25 °C, DMSO-d_6/D_2O 1:1 v/v) and FT-IR spectra were performed to characterize the conjugate, and the amount of bound Chl in CS-Chl conjugate was determined by measuring the absorbance of a DMSO solution of CS-Chl (5 mg mL^{-1}) at 306 nm by using a calibration curve of free Chl in DMSO (32.8–328 μM).

2.3. Determination of the critical aggregation concentration (CAC)

The critical aggregation concentration (CAC) of CS-LA and CS-Chl in aqueous solution was calculated using pyrene as a nonpolar probe, by virtue of its property to modify its fluorescence signal when located inside or in the proximity of the micelles hydrophobic core (Curcio et al., 2021). Briefly, 20.0 μL pyrene solution in acetone (3.0×10^{-5} M) were evaporated in vials. In separate experiments, each conjugate was dissolved at various concentrations in phosphate buffer under magnetic stirring and then added to the pyrene vials. The contents of the vials were mixed for 12 h, thereby leading to solutions with pyrene concentration of ca. 6.0×10^{-7} M. Then, the intensity ratios (I_3/I_1) of the third vibronic band at 385 nm to the first one at 373 nm of the fluorescence emission spectra of pyrene were recorded at 25 °C. Pyrene fluorescence emission spectra (λexc = 336 nm; λem = 350–500 nm) were recorded on Hitachi F-2500 spectrometer (Tokyo, Japan).

All chemicals were purchased from Merck/Sigma Aldrich, Germany.

2.4. Preparation of nanoparticle formulations

CS-LA and CS-Chl were dissolved in 10 mL THF in a 50 mL round bottomed flask to reach a final concentration of 1 mg mL^{-1}. Next, 5 mL phosphate buffer (0.01 M, pH 7.4) were quickly added and vortexed for 2 min at 200 rpm. THF was evaporated using a rotary evaporator (40 rpm, 40 °C, 10 min), yielding the colloidal system (LCPs) with a final concentration of 1 mg mL^{-1}. DOX loaded nanoparticles (DOX@LCPs) were prepared as described above, by adding 5 mL DOX solution (30 μM) in phosphate buffer (0.01 M, pH 7.4) to the conjugates solution in THF. The DOX encapsulation efficiency was calculated transferring 5 mL DOX@LCPs into a dialysis bag (Spectra/Por, MWCO 3.5 kDa, Spectrum, Canada) immersed in 25 mL of phosphate buffer (0.01 M, pH 7.4). The dialysis was stopped after 1 h, when no drug was detected in the recipient solution. Then, 3 mL of purified and non-purified nanoparticles were diluted with 25 mL methanol, in order to break the polymeric structures, and DOX concentration was measured by UV–Vis spectrophotometer (Evolution 201 spectrophotometer, ThermoFisher Scientific, Hillsboro, OR, USA) using a standard calibration curve of DOX (0.6–3.0 μM) in phosphate buffer (0.01 M, pH 7.4).

Size distribution of LCPs and DOX@LCPs was determined using a 90 Plus Particle Size Analyzer DLS equipment (Brookhaven Instruments Corporation, New York, USA) at 25 °C. The autocorrelation function was measured at 90° and the laser beam operated at 658 nm. The polydispersity index (PDI) was directly obtained from the instrumental data fitting procedures by the inverse Laplace transformation and Contin methods. PDI values ≤0.3 indicate homogenous and mono-disperse populations (Provencher, 1982).

Z-potential (ζ) was measured by laser Doppler electrophoretic mobility measurements using a Zetasizer Nano ZS instrument (Malvern Instruments Ltd., Malvern, U.K.), at 25.0 ± 0.1 °C (t = 0 and 14 days). All analyses were done in triplicate. Z-potential values and standard deviations were elaborated directly from the instrument. Morphological analysis of LCPs was carried out using transmission electron microscopy (TEM; HRTEM/Tecnai F30 [80 kV] FEI company, Hillsboro, OR, USA). A drop of the nanoparticles dispersion was placed on a Cu TEM grid (200 mesh, Plano GmbH, Wetzlar, Germany), and the sample in excess was removed using a piece of filter paper. A drop of 2% (*w/v*) phosphotungstic acid solution was then deposited on the carbon grid and left to stay for 2 min. Once the excess of staining agent was removed with filter paper, the samples were air-dried and the thin film of stained nanoparticles was observed.

All chemicals were purchased from Merck/Sigma Aldrich, Germany.

2.5. In vitro release studies

Release experiments from LCPs and DOX@LCPs were carried out by means of the dialysis method under sink conditions. For LCPs sample, 2 mL suspension were loaded in a dialysis bag (Spectra/Por, MWCO 3.5 kDa, Spectrum, Canada) and dialyzed against 20 mL phosphate buffer (0.01 M, pH 7.4) containing esterase from porcine liver at different concentrations (0 and 50 U mL^{-1}) at 37 °C in a beaker with constant stirring. At pre-established times, samples (2 mL) of release medium were withdrawn, replaced with fresh medium and analyzed by a UV–Vis spectrophotometry using a standard calibration curve of Chl (32.8–164 μM) in phosphate buffer (0.01 M, pH 7.4). Similarly, release experiments from DOX@LCPs were carried out loading 2 mL of LCPs suspension in a dialysis bag (Spectra/Por, MWCO 3.5 kDa, Spectrum, Canada) and using an equal volume (20 mL) of phosphate buffer (0.01 M, pH 7.4) containing GSH at different concentrations (0 and 10 mM) as release media at 37 °C in a beaker with constant stirring. At pre-established times, 2 mL of release medium were withdrawn, replaced with fresh medium and analyzed by UV–Vis spectrophotometry using a standard calibration curve of DOX (0.6–3.0 μM) prepared under the same conditions. Monitoring of dialysis experiments was carried out by recording the UV–Vis spectra in the wavelength range 240–400 (Chl) and 350–550 (DOX) nm. All the spectral data stored for each dialysis were arranged in a matrix D_{ri} (n,m), where n spectra recorded at selected times were described by m wavelength variables. The experimental data were processed by the chemometric methodology, applying the multivariate curve resolution-alternating least squares algorithm (MCR-ALS) (De Luca et al., 2022). Multivariate resolution of the data was able to evaluate the release profile of Chl and DOX discriminating the spectral information due to the drugs and background, individually. Quantitative assaying of the two drugs was possible by selecting the specific "calibration" and "non-negativity" constraints in the MCR-ALS iterative elaboration; for this purpose, the augmented matrices were built, each consisting of two subsets, with data from pure drug calibration spectra and the subset of the data acquired in the respective dialysis experiments (De Luca et al., 2017). MCR-ALS toolbox (version 2) were used in Matlab® environment (The Mathworks, Inc., MA, USA) (Jaumot et al., 2015).

At each experimental time, the drug released was expressed as the ratio (M_t/M_0) between the amount of drug recovered in solution (M_t) and that loaded into the LCPs systems (M_0).

All chemicals were purchased from Merck/Sigma Aldrich, Germany.

2.6. Cell culture testing

For in vitro testing the human triple-negative breast cancer cell line, MDA-MB-231, was kindly provided by Associate Professor Caroline Ford from the School of Women's and Children's Health at the Lowy Cancer Research Centre, UNSW Sydney. MDA-MB-231 cells were cultured in DMEM, containing 2 mM L-glutamine (Gibco, Massachusetts, USA) and 10% fetal bovine serum (FBS) (Sigma, Massachusetts, USA) and incubated in a humidified incubator with 5% CO_2 at 37 °C. For testing the viability, cells were seeded in transparent 96 well plates at 5×10^3 cells/well and left growing for 24 h before addition of freshly diluted drug or control. Media was replaced after 24 h with Alamar Blue reagent and incubated for a further 3–6 h for reduction by active mitochondria, before spectrophotometry measurement at 470-495 nm.

2.7. Statistical analysis

Experiments were performed in triplicate and the results agreed within the relative standard deviation. For biological tests, one-way analysis of variance was performed to assess the significance of the differences among data, and Tukey-Kramer post-test was used to compare the data from different treatments ($P < 0.05$ was considered statistically significant).

3. Results and discussion

3.1. Synthesis and characterization of CS-Chl and CS-LA conjugates

CS functional derivatives to be employed as components of stimuli-responsive drug delivery systems were synthesized by covalent attachment of Chl and LA to the polysaccharide backbone by EDC-mediated esterification reactions. The novelty and aims of our approach are summarized below: i) to improve the poor pharmacokinetic properties of Chl (low solubility, rapid degradation in aqueous media, as well as severe side effects) by conversion into a polymeric prodrug specimen sensitive to the esterase activity; ii) to confer redox-responsiveness to the final carrier by exploiting the LA dithiolane nucleus as a GSH substrate; iii) to endow CS with self-assembling properties allowing the preparation of polymeric nanoparticles.

Both functional conjugates were characterized by ^{1}H NMR, FT-IR spectra, and determination of Critical Aggregation Concentration (CAC), while UV–Vis spectroscopy methods were employed to calculate the derivatization degree of each esterification product.

In ^{1}H NMR spectrum of CS-Chl conjugate (derivatization degree of 76 mg Chl per gram of conjugate as per UV–Vis analyses), the typical signal of CS acetyl protons (1.77 ppm, $H_{a'}$) and aromatic protons of Chl at 6.70 (H_e) and 6.99 (H_f) ppm can be observed (Fig. 2A). Conversely, the FT-IR spectrum of the same sample exhibited CS absorption bands at 1650 and 1014 cm-1, indicative of the amide carbonyl (C=O) and C—O

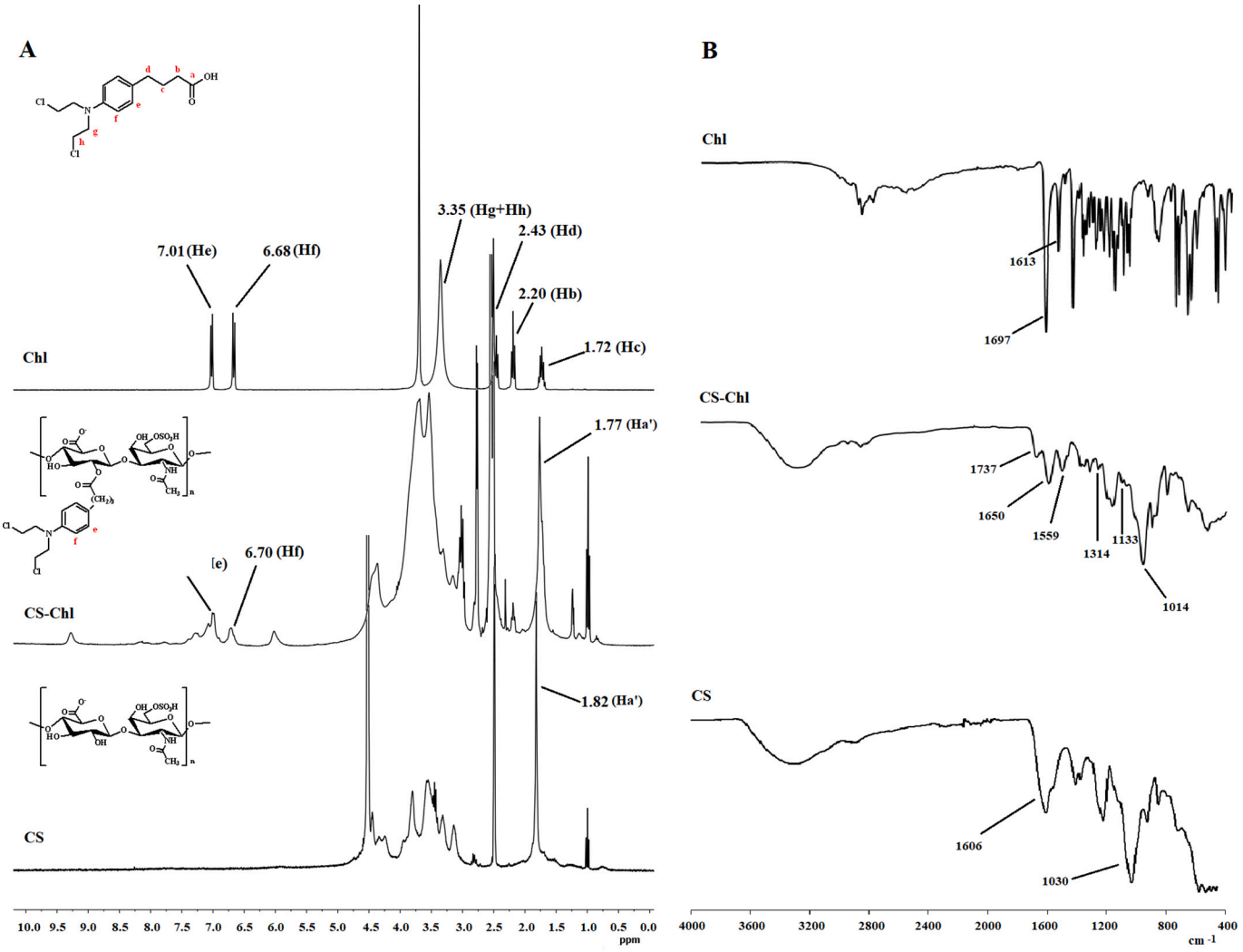

Fig. 2. (A) ^{1}H NMR and (B) FT-IR spectra of Chl, CS-Chl and CS samples.

stretching vibrations of the polysaccharide, respectively(Foot and Mulholland, 2005), and the appearance of the signal at 1737 attributable to the C═O stretching of newly formed ester functionalities. Moreover, the stretching vibration of Chl aromatic and CH_2 (CH_2Cl) wagging were detected at 1559 and 1314 cm^{-1}, respectively (Fig. 2B).

Similarly, to CS-Chl, the ^1H NMR and FT-IR analyses of CS-LA conjugate (LA derivatization degree of 10 mg per gram of conjugate as per Ellman's test) confirmed the successful conjugation. In ^1H NMR spectrum, in addition to the CS acetyl protons signals at 1.77 ppm, the LA peaks at 1.64 and 2.92 ppm, attributable to the overlapped multiplets of the CH_2 protons of the aliphatic and to that of the dithiolane nucleus (H_h), respectively, were recognized (Fig. 3A).

The FT-IR spectrum revealed a broad absorption band ranging from 1727 to 1534 cm^{-1} resulting from the overlapping of the stretching vibrations of the newly formed ester carbonyl group and the CS amide carbonyl group, while new signals at 1097 and 1138 cm^{-1} were ascribable to the C-O-C stretching vibrations (ester group) (Fig. 3B).

As above mentioned, the CS-Chl and CS-LA amphiphiles were also characterized in terms of self-assembling behaviour by determining the CAC, intended as the concentration value above which they can form micellar structures. This parameter, calculated using pyrene as fluorescent probe, is an important indicator of the stability of the micelles under high dilution conditions (such as in vivo conditions): low CAC values correspond to greater ability to form self-assembling structures at low concentrations. Plotting the dependence of pyrene fluorescence signals (I_{385}/I_{373} ratio) vs the logarithm of conjugate concentration, the onset of self-assembly was identified at the concentration point where a sharp change of the fluorescence intensity was observed. CAC values of 0.063 and 0.26 μg mL^{-1} were recorded for CS-Chl and CS-LA, respectively (Fig. 4A). The much lower CAC value obtained for CS-Chl vs CS-LA is in accordance with the higher derivatization degree (76 vs 10 mg g^{-1}) that, reducing the hydrophilic/lipophilic balance, improved the self-assembling and the stability properties of the conjugate.

3.2. Synthesis and characterization of LCPs and DOX@LCPs self-assembling nanoparticles

Dual enzyme/redox-responsive self-assembling nanoparticles were prepared by combining CS-Chl and CS-LA conjugates by water addition/solvent evaporation technique, a well-known methodology for the preparation of self-assembling polymeric nanoparticles (Marsden et al., 2010) successfully used in our previous works for promoting the self-assembling of lipidized natural polymers such as keratin and gelatin (Curcio et al., 2015a; Curcio et al., 2015b). Briefly, a phosphate buffer solution (pH 7.4) was added to a THF solution of the amphiphilic polymers, and the subsequent removal of the organic solvent resulted in a decrease of the solubility of the amphiphiles, thus leading to their organization, by self-assembling phenomena, in a structure where the conjugates hydrophobic moieties (Chl and LA) formed the inner structure, and the CS hydrophilic portions were oriented towards the aqueous regions (Fig. 1).

TEM micrographs of negatively stained LCPs, combined with DLS analysis, showed spherical nanoparticles (Fig. 4B) with a mean hydrodynamic diameter and P.D.I. of 45 nm and 0.24 (Fig. 4C), respectively,

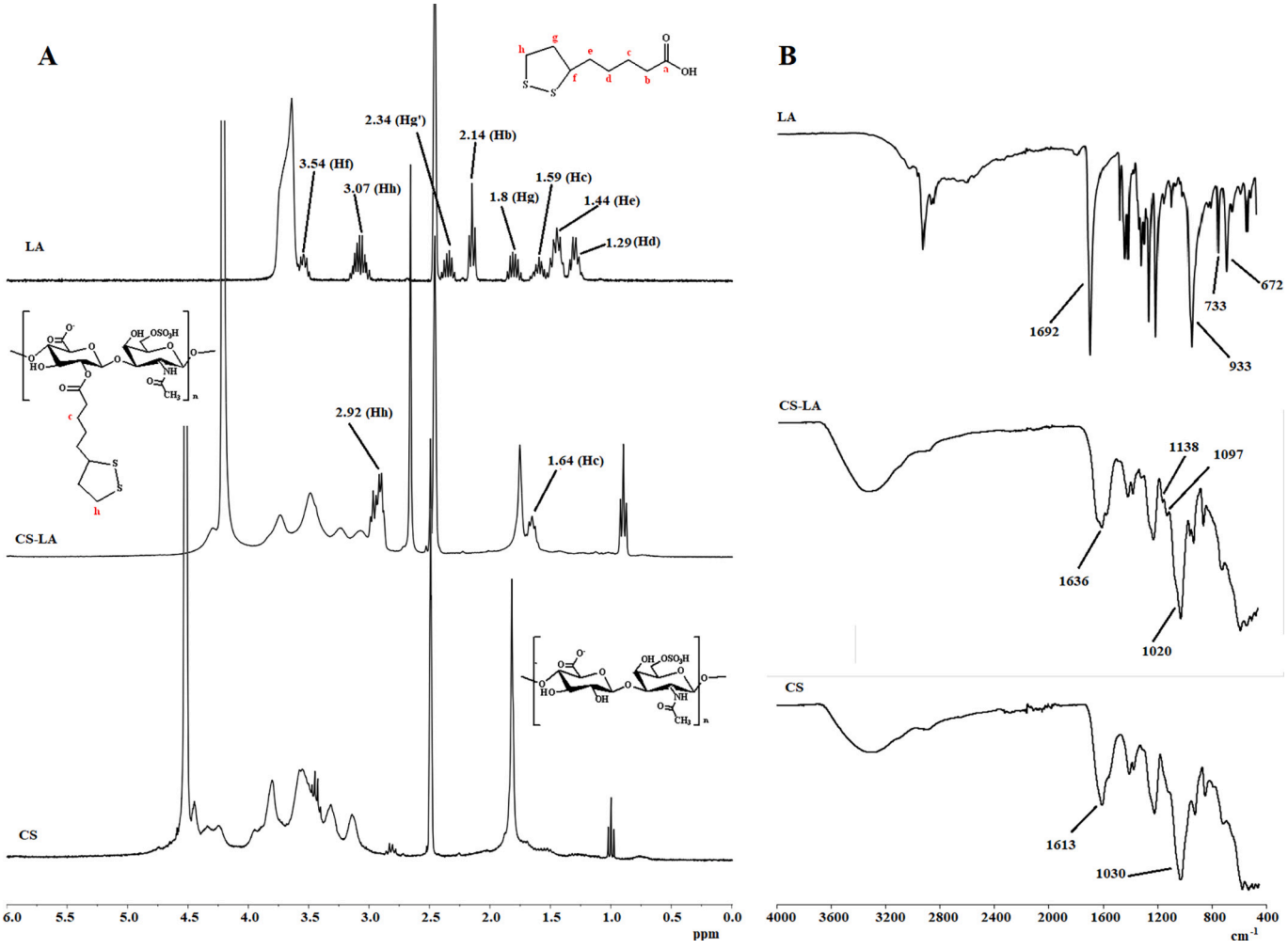

Fig. 3. (A) ^1H NMR and (B) FT-IR spectra of LA, CS-LA and CS samples.

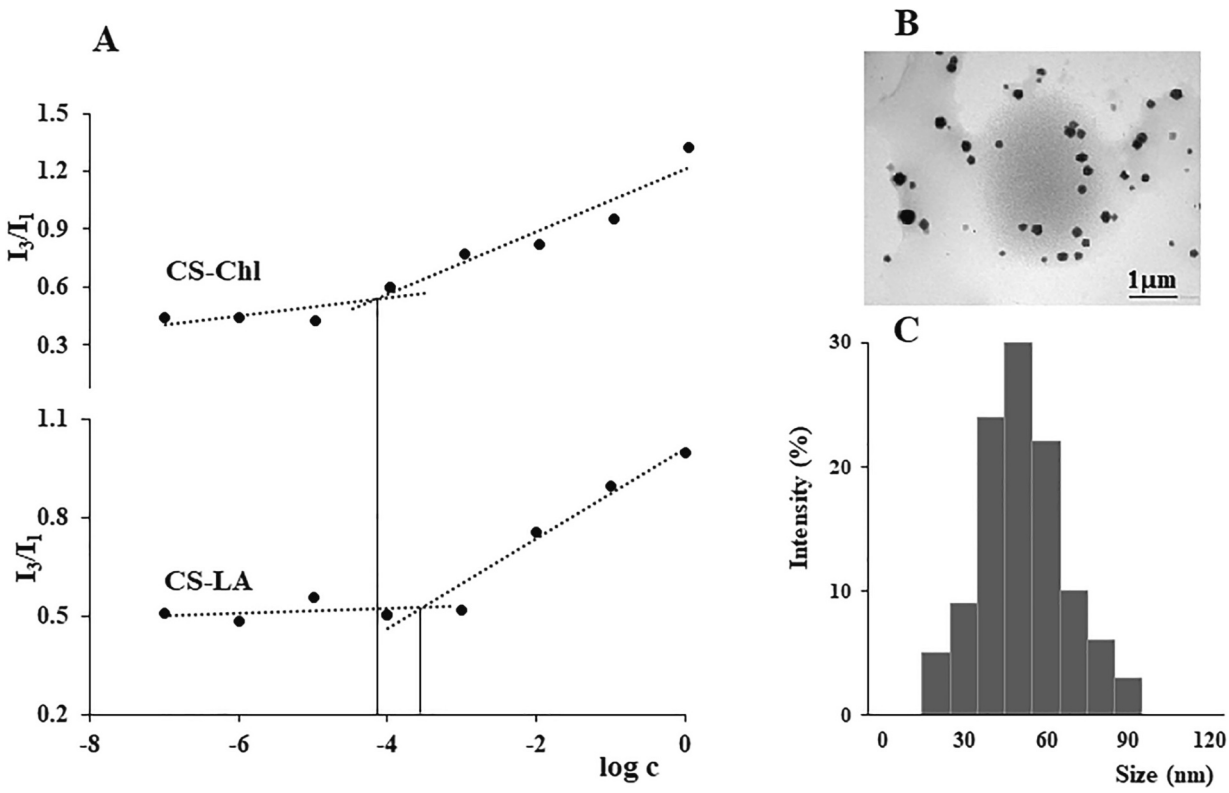

Fig. 4. (A) CAC determination of CS-Chl and CS-LA by pyrene fluorescence method at pH 7.4; (B) TEM image of negatively stained LCPs and (C) dimensional distribution of LCPs by DLS analysis.

confirming the suitability of the proposed procedure for the obtainment of nanoparticles for cancer treatment (Tang et al., 2014). Nanosystem dispersion was characterized by a ζ-potential value of - 44 mV, remaining almost unchanged over 14 day time at 25 °C, demonstrating the high stability of the formulation since it is widely recognized that colloidal systems with ζ-potential $> +30$ mV and < -30 mV are electrically stabilized (Chiesa et al., 2018).

Moreover, stability tests were also performed in the presence of HSA, simulating plasma environment. Reports suggest that the stability in plasma is a key issue to be assessed because it greatly affects the nanoparticle cellular uptake or the rate and extent of release of loaded therapeutic agents (Prabha et al., 2002). Upon intravenous administration, indeed, nanoparticle systems undergo surface interactions with serum proteins, creating a protein corona that may cause nanoparticle aggregation/destabilization or even elicit an immune response (Suvarna et al., 2018). The effect of protein binding on the hydrodynamic size was investigated after 24 h incubation to allow the protein to nanoparticle interaction equilibration to be completed. The results showed that no significant variations in the size of LCPs were recorded over a 7 days period of time, suggesting a negligible interaction with plasma protein. This was expected due to the anionic nature of both LCPs and HSA in physiological conditions, promoting the establishment of electrostatic repulsion forces (Najer et al., 2022).

To verify the capability of the proposed nanoparticles to vectorize therapeutic agents, DOX was loaded during the LCPs formation by solubilization in the phosphate buffer solution, obtaining the DOX@LCPs sample with an encapsulation degree of 93%. The high encapsulation degree can be ascribable to the strong affinity of the drug towards the nanoparticles components due to the presence, at pH 7.4, of strong electrostatic interactions between the protonated form of drug (pKa of 9.93 (Guo et al., 2018)) and the anionic CS, as well as to the formation of hydrogen bonds, Van der Waals forces, and hydrophobic interactions.

3.3. In-vitro release experiments from LCPs and DOX@LCPs

The proposed LCPs and DOX@LCPs were designed to specifically respond to two of the most common pathological stimuli from cancer cells, the esterase overexpression and the redox potential, triggering the Chl and DOX release in a spatial pattern and avoiding the drug leakage in blood and healthy cells.

To demonstrate the esterase-responsivity, Chl release experiments from LCPs were performed in media mimicking physiological (phosphate buffer, pH 7.4) and intracellular (esterase 50 UE mL^{-1})

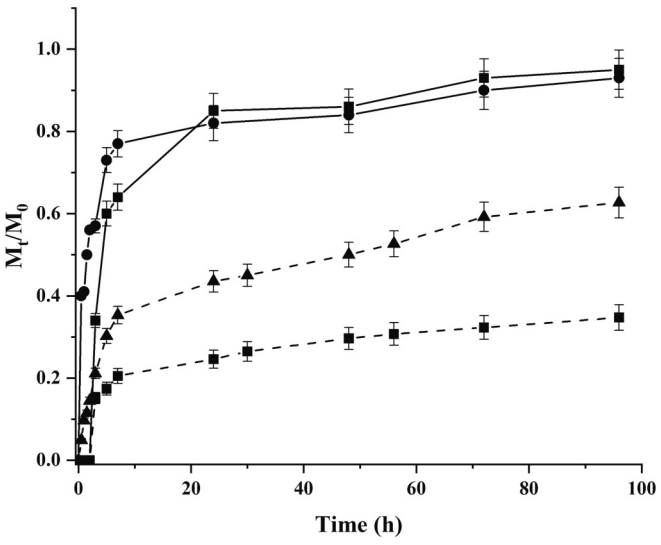

Fig. 5. Release profiles calculated by MCR-ALS modelling of Chl (solid lines) in phosphate buffer at pH 7.4 (–■-) and esterase 50 U mL^{-1} (–●-) and DOX (dashed lines) in phosphate buffer at pH 7.4 (–■-) and GSH 10 mM (–▲-).

environments (Fig. 5). Sustained Chl release profiles were observed in both media, as a consequence of the conjugation to CS and subsequent incorporation into the polymeric structure. More in detail, in the absence of the enzyme, the release started after 2 h incubation, raising 64% after 7 h, while in the enzyme-containing medium, a more rapid delivery pattern was recorded due to the esterase hydrolytic activity, with a burst release of 41% in 0.5 h, becoming 77% after 7 h.

Furthermore, the nanoparticle destabilization in the reducing medium, and the consequent triggered drug release, was proved by analysing the DOX release experiments in phosphate buffer at pH 7.4 and GSH 10 mM. The release profile from DOX@LCPs was found to be prolonged over time due to the strong drug-carrier affinity, with negligible release percentages till 2 h incubation, and not exceeding 35% after 96 h. On the contrary, when GSH was added, a relevant increase in the release values was recorded, raising almost 60% after 72 h. This behaviour can be related to the reduction of disulfide bridges that, modifying the structural arrangement in the LCPs, perturbed the DOX-nanoparticle interaction forces, thus promoting the drug release. On the other hands, it is well-known that the insertion of GSH in the release media reduced the pH to 5.5, with a modification of the DOX protonation degree. Thus, to assess the effect of the pH variation, further release experiments were performed at this pH value (Fig. S1). The results showed that DOX protonation was responsible for more significant electrostatic interaction with the polymeric structure (M_t/M_0 values not exceeding 15% even after 96 h of incubation), further confirming that the increase of the DOX release upon GSH exposure was a direct consequence of the nanoparticle destabilization.

For better analysing the mechanism involved in the Chl and DOX releases, we applied suitable kinetic models available in the literature, namely the zero-order (Eq. 1), first-order (Eq. 2), Ritger-Peppas (Eq. 3) and Peppas-Sahlin (Eq. 4) models:

$$\text{Zero} - \text{order} \qquad \frac{M_t}{M_0} = k_0 t \tag{1}$$

$$\text{First} - \text{order} \qquad \frac{M_t}{M_0} = c\left(1 - e^{-k_1 t}\right) \tag{2}$$

$$\text{Peppas} - \text{Sahlin} \qquad \frac{M_t}{M_0} = k' t^m + k'' t^{2m} \tag{3}$$

Where k_0, k_1, k', and k'' were the zero-order, first-order, Fickian diffusion, and anomalous diffusion kinetic constants; c the first order release coefficient, m the Peppas-Sahlin coefficient, and t the releasing time. It should be pointed out that, for both drugs, the modelling at pH 7.4 was performed using the experimental data at $t > 2$ h, since lower incubation times were characterized by negligible drug release, and thus considered as pre-incubation times needed for the external stimuli to become effective.

The obtained kinetic parameters were collected in Table 1 together with the indication of α (Eq. 4), β' (Eq. 5), and β'' (Eq. 6) ratios calculated as follows:

$$\alpha = \frac{k'}{k''} \tag{4}$$

$$\beta' = \frac{k'_{St}}{k'_{7.4}} \tag{5}$$

$$\beta'' = \frac{k''_{St}}{k''_{7.4}} \tag{6}$$

Where k'_{St}, k''_{St} are the k' and k'' values recorded under stimulus (Esterase or GSH), while $k'_{7.4}$, $k''_{7.4}$ are the k' and k'' values recorded under physiological (pH 7.4) conditions.

It is clearly evident that the release of both drugs is not a steady state phenomenon (Malekjani and Jafari, 2021), since the zero-order equation (Eq. 1) was not suitable for fitting the experimental data ($R^2 < 0.80$ in all cases). On the other hands, the possibility to apply the first order model (Eq. 2, $R^2 > 0.90$) to the Chl release suggested that the concentration gradient between the carrier to the external media phases could be responsible for the drug release (Malekjani and Jafari, 2021). More information can be obtained when the Peppas-Sahlin model was applied to evaluate the Fickian and anomalous contribution of the diffusion of the drug to the releasing media (Unagolla and Jayasuriya, 2018). Here, the involvement of the enzymatic cleavage resulted in an enhancement of the Chl release rate with respect to physiological conditions (increase of both k' and k'' values), with the anomalous contribution becoming more relevant as underlined by the higher β'' compared to β' (value).

When considering the DOX release, the high drug to carrier affinity should be considered to explain the release mechanism. At physiological pH, the experimental data can be only fitted by the Peppas-Sahlin equation, indicating that the driving force of the release is the diffusion of the drug from the carrier to the releasing media. The application of the redox stimulus destabilized the carrier structure, thus lowering the ability of the carrier to effectively retain the drug, and the release became faster ($\beta' > 1.0$) and closer to a Fickian diffusion ($\beta'' < 1.0$). This statement was confirmed by considering the DLS analyses upon exposure the GSH 10 mM, showing increased values of hydrodynamic diameter (154 nm) and PDI (0.47). This can be used as a prove of the effective LCPs destabilization due to the reduction of the LA disulfide bridges by GSH.

The results of release experiments from LCPs, namely the possibility to speed up the Chl release rate after 0.5 h incubation in esterase-containing medium, together with the enhancement of the amount of released DOX upon exposure to high GSH conditions, allowed hypothesizing the improvement of biological activity of a Chl-DOX combination therapy due to a selective accumulation of both drugs within the tumour site. The ultimate aim of an effective smart delivery vehicle, indeed, is not yet to prolong the release over time, but to vectorize the drugs to the tumour site minimizing the leaking of the payloads within the systemic circulation (Liu et al., 2016).

3.4. Biological characterization

Chlorambucil, a DNA alkylating agent, is a first line chemotherapeutic drug for the treatment of chronic lymphocytic leukemia and lymphomas, as well as for aggressive and drug-resistant tumors, such as triple negative breast cancer and pancreatic adenocarcinomas (Di Antonio et al., 2014; Millard et al., 2013). The presence of two reactive

Table 1
Kinetic parameters for Chl and DOX release from LCPs.

Drug	Release medium	Zero order		First order		Peppas-Sahlin						
		R^2	k_0 (10^{-2})	R^2	k_1 (10^{-1})	R^2	m	k' (10^{-1})	k'' (10^{-2})	α	β'	β''
Chl	7.4	0.6317	1.70	0.9676	3.68	0.9780	0.34	4.59	5.77	7.95	1.20	1.48
	Esterase	0.4673	1.69	0.9032	6.43	0.9722	0.31	5.49	8.54	6.43		
DOX	7.4	0.7635	0.50	0.8673	3.37	0.9965	0.14	1.09	3.70	2.95	1.23	0.19
	GSH	0.7999	0.87	0.9493	1.61	0.9683	0.45	1.34	0.72	18.6		

chloroethyl side chains allows the interaction with nucleic acids, proteins and phospholipids, effectively decreasing the amount of drug at the target site. This non-specific reactivity, together with the slow cell internalization, remarkably reduces its therapeutic potency, requiring the administration of high doses (Fan et al., 2015). Moreover, the severe side effects, including myelotoxicity and neurotoxicity, are limiting factors for its effective employment, asking for the development of new therapeutic tools, such as self-assembling prodrugs (Liu et al., 2017).

Here, we evaluated the LCPs antitumor efficacy in MDA-MB-231 triple negative breast cancer cell line, compared to the free Chl at the same equivalent concentrations (Fig. 6). Free Chl was found to be almost ineffective in killing cancer cells, while a significant anti-cancer activity was recorded upon conjugation to the nanoparticle system, with viability percentages ranging from almost 80 to 40% enhancing the drug equivalent concentration, potentially as a consequence of the improved drug uptake. This statement was proved by confocal microscopy analyses, where a complete and fast uptake of the FITC-labeled nanoparticle systems was observed (Fig. 7). On the other hands, the high esterase and GSH intracellular concentrations, triggering the prodrug hydrolysis and nanoparticle destabilization, enhanced the Chl availability within the target site, significantly improving the anticancer activity with respect to the free form of the drug (cell viability values decreasing from 89 to 38% for free and conjugated Chl at 7.6 μg mL^{-1}, respectively).

Moreover, as before discussed, the ability of the proposed prodrug to self-assembly in nanoparticle systems was exploited for the encapsulation of a second chemotherapeutic agent (i.e. DOX) with the development of a combination protocol, since it is well known that the treatment of several cancer types benefit from the simultaneous administration of cytotoxic drugs working with different mechanism of action (Gilad et al., 2021; Jaaks et al., 2022).

The combination of free drugs carried out to an anticancer activity comparable to that obtained when DOX was used as a single treatment because of the above discussed poor ability of Chl to enter cancer cells.

Then, a selected amount of DOX (2.0 μg mL^{-1}) was encapsulated into CLPs used at the previously tested equivalent Chl concentrations (1.9, 3.8, and 7.6 mg μL^{-1}) (Fig. 6). The results showed a significant reduction of cell viability up to 95%, as a result of an enhanced drug uptake within cells (see confocal microscopy experiments). Although further experiments are being performed to underline the biological mechanisms at the basis of the enhanced cytotoxic activity, including the possibility to reverse the multi-drug resistance mechanisms, the results confirmed the high potency of the proposed nanoformulation for the treatment of highly aggressive cancer cells.

4. Conclusion

To address the need for vectorizing cytotoxic agents (Chl and DOX) to cancer cells, we explored the stimuli-responsive approach as a valuable and effective strategy. To this aim, chondroitin sulfate (CS) was selected as base materials for the obtainment of self-assembling conjugates endowed with redox- and esterase-sensitive functionalities. The redox-responsivity was conferred by the insertion of LA groups, while the covalent coupling of Chl was used to obtain an esterase-responsive prodrug. The nanoparticle destabilization within the cancer environments was found to trigger the release of the bioactive agents, with the esterase and GSH activities being able to enhance the Chl and DOX release, respectively. The nanoparticles were able to enhance the anticancer activity of the two drugs against MDA-MB-231 cells by means of enhanced cell internalization, and can thus represent a promising tool for an effective treatment of highly aggressive solid cancers.

Research funding

This work was supported by PON R&I 2014–2020 - ARS01_00568 - SI.F.I.PA.CRO.DE. – Sviluppo e industrializzazione farmaci innovativi per terapia molecolare personalizzata PA. CRO.DE. M.C. is funded by

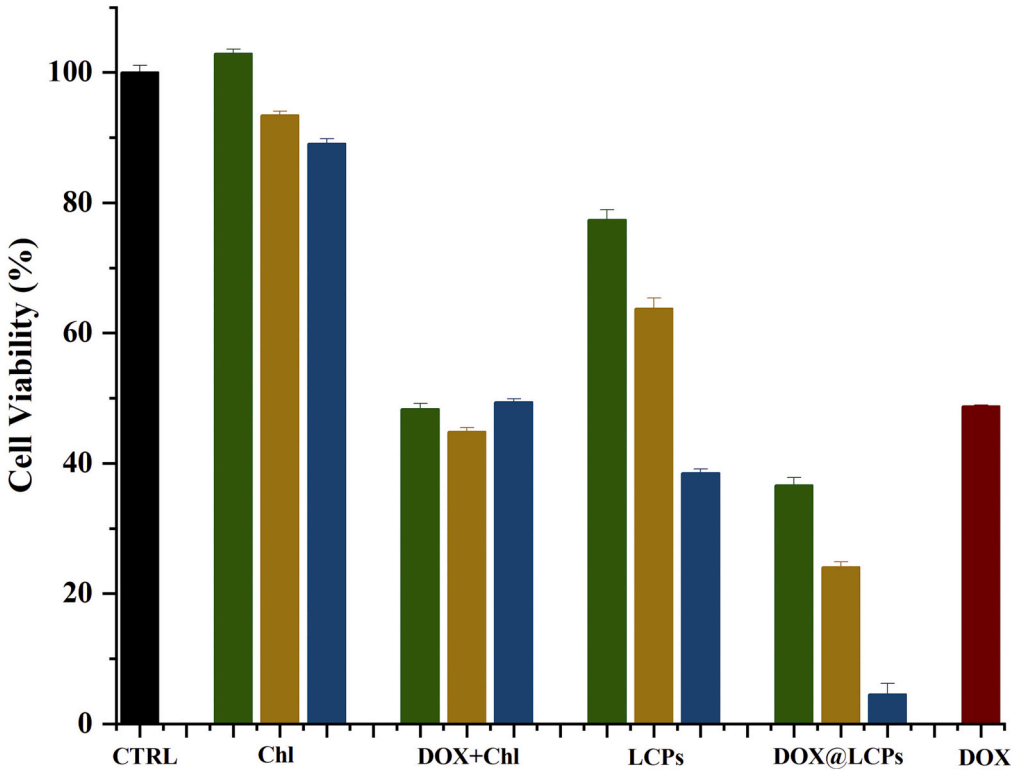

Fig. 6. MDA-MB-231 viability after 48 h exposure to free Chl, Chl + DOX, LCPs, and DOX@LCPs at Chl equivalent concentrations of 1.9 (green bars), 3.8 (dark yellow bars), and 7.9 (blue bars) μg mL^{-1}. The DOX concentration is 2.0 μg mL^{-1} in each treatment. (For interpretation of the references to colour in this figure legend, the reader is referred to the web version of this article.)

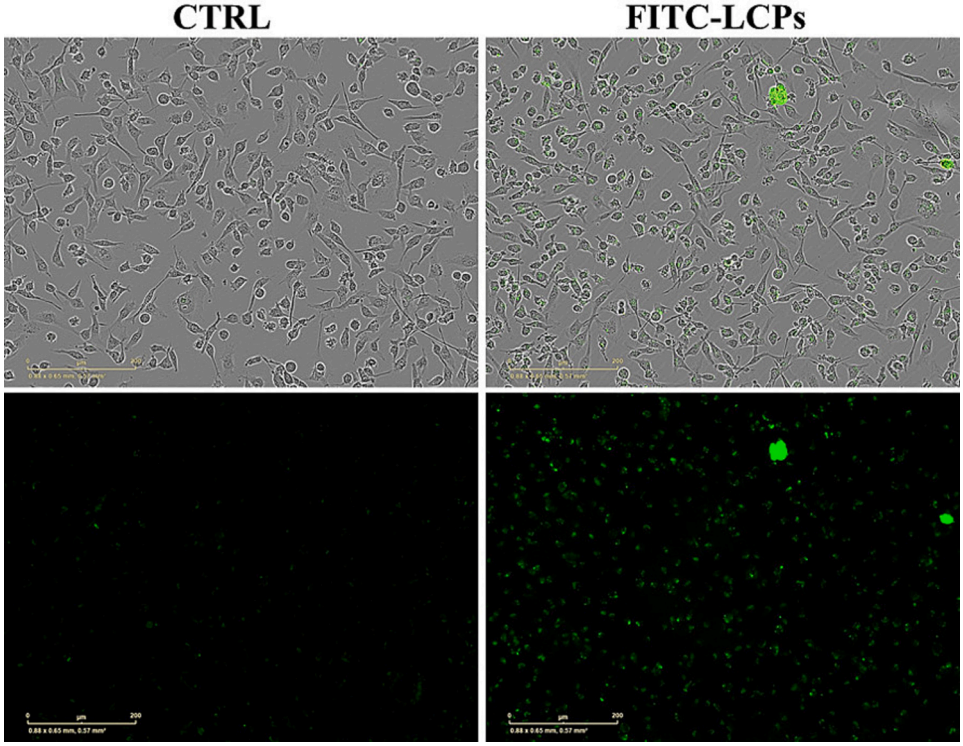

Fig. 7. Confocal images of MDA-MB-231 cell exposed to FITC-LCPs (3.8 μg mL^{-1}) for 24 h.

PON R&I 2014–2020 Azione IV.6 – "Contratti di ricerca su tematiche Green".

CRediT authorship contribution statement

Ensieh Poursani: Formal analysis, Investigation. **Giuseppe Cirillo:** Investigation, Validation, Writing – review & editing. **Manuela Curcio:** Conceptualization, Validation, Visualization, Writing – original draft. **Orazio Vittorio:** Data curation, Methodology, Validation, Writing – review & editing. **Michele De Luca:** Investigation, Methodology, Writing – review & editing. **Antonella Leggio:** Investigation, Methodology, Writing – review & editing. **Fiore Pasquale Nicoletta:** Funding acquisition, Supervision, Writing – review & editing. **Francesca Iemma:** Funding acquisition, Supervision, Writing – review & editing.

Declaration of competing interest

The authors declare the following financial interests/personal relationships which may be considered as potential competing interests:

Manuela Curcio reports financial support was provided by Government of Italy Ministry of Education University and Research.

Data availability

Data will be made available on request.

Appendix A. Supplementary data

Supplementary data to this article can be found online at https://doi.org/10.1016/j.ijpx.2024.100235.

References

Baghba, R., Roshangar, L., Jahanban-Esfahlan, R., Seidi, K., Ebrahimi-Kalan, A., Jaymand, M., Kolahian, S., Javaheri, T., Zare, P., 2020. Tumor microenvironment complexity and therapeutic implications at a glance. Cell Commun. Signal 18.

Barclay, T.G., Day, C.M., Petrovsky, N., Garg, S., 2019. Review of polysaccharide particle-based functional drug delivery. Carbohydr. Polym. 221, 94–112.

Brindisi, M., Curcio, M., Frattaruolo, L., Cirillo, G., Leggio, A., Rago, V., Nicoletta, F.P., Cappello, A.R., Iemma, F., 2022. CD44-targeted nanoparticles with GSH-responsive activity as powerful therapeutic agents against breast cancer. Int. J. Biol. Macromol. 221, 1491–1503.

Chiesa, E., Dorati, R., Conti, B., Modena, T., Cova, E., Meloni, F., Genta, I., 2018. Hyaluronic Acid-decorated Chitosan Nanoparticles for CD44-Targeted delivery of Everolimus. Int. J. Mol. Sci. 19, 2310.

Curcio, M., Blanco-Fernandez, B., Diaz-Gomez, L., Concheiro, A., Alvarez-Lorenzo, C., 2015a. Hydrophobically Modified Keratin Vesicles for GSH-Responsive Intracellular Drug Release. Bioconjug. Chem. 26, 1900–1907.

Curcio, M., Cirillo, G., Vittorio, O., Spizzirri, U.G., Iemma, F., Picci, N., 2015b. Hydrolyzed gelatin-based polymersomes as delivery devices of anticancer drugs. Eur. Polym. J. 67, 304–313.

Curcio, M., Paoli, A., Cirillo, G., Di Pietro, S., Forestiero, M., Giordano, F., Mauro, L., Amantea, D., Di Bussolo, V., Nicoletta, F.P., Iemma, F., 2021. Combining Dextran Conjugates with Stimuli-Responsive and Folate-Targeting activity: a New Class of Multifunctional Nanoparticles for Cancer Therapy. Nanomaterials 11, 1108.

De Luca, M., Ioele, G., Spatari, C., Ragno, G., 2017. A single MCR-ALS model for drug analysis in different formulations: Application on diazepam commercial preparations. J. Pharm. Biomed. 134, 346–351.

De Luca, M., Occhiuzzi, M.A., Rizzuti, B., Ioele, G., Ragno, G., Garofalo, A., Grande, F., 2022. Interaction of letrozole and its degradation products with aromatase: chemometric assessment of kinetics and structure-based binding validation. J. Enzym. Inhib. Med. Ch. 37, 1600–1609.

Di Antonio, M., McLuckie, K.I.E., Balasubramanian, S., 2014. Reprogramming the Mechanism of Action of Chlorambucil by Coupling to a G-Quadruplex Ligand. J. Am. Chem. Soc. 136, 5860–5863.

Dong, H.N., Pang, L., Cong, H.L., Shen, Y.Q., Yu, B., 2019. Application and design of esterase-responsive nanoparticles for cancer therapy. Drug Deliv. 26, 416–432.

Dzobo, K., Senthebane, D.A., Dandara, C., 2023. The Tumor Microenvironment in Tumorigenesis and Therapy Resistance Revisited. Cancers 15, 376.

Fan, M.L., Liang, X.F., Li, Z.H., Wang, H.Y., Yang, D.B., Shi, B.Z., 2015. Chlorambucil gemcitabine conjugate nanomedicine for cancer therapy. Eur. J. Pharm. Sci. 79, 20–26.

Foot, M., Mulholland, M., 2005. Classification of chondroitin sulfate a, chondroitin sulfate C, glucosamine hydrochloride and glucosamine 6 sulfate using chemometric techniques. J. Pharm. Biomed. 38, 397–407.

Gilad, Y., Gellerman, G., Lonard, D.M., O'Malley, B.W., 2021. Drug Combination in Cancer Treatment-from Cocktails to Conjugated Combinations. Cancers 13, 669.

Guo, X., Cheng, Y., Zhao, X., Luo, Y., Chen, J., Yuan, W.E., 2018. Advances in redox-responsive drug delivery systems of tumor microenvironment. J. Nanobiotech. 16, 74.

He, Q.Y., Chen, J., Yan, J.H., Cai, S.D., Xiong, H.J., Liu, Y.F., Peng, D.M., Mo, M., Liu, Z. B., 2020. Tumor microenvironment responsive drug delivery systems. Asian J. Pharm. Sci. 15, 416–448.

Huda, S., Alam, M.A., Sharma, P.K., 2020. Smart nanocarriers-based drug delivery for cancer therapy: an innovative and developing strategy. J. Drug. Deliv. Sci. Tec. 60, 102018.

Jaaks, P., Coker, E.A., Vis, D.J., Edwards, O., Carpenter, E.F., Leto, S.M., Dwane, L., Sassi, F., Lightfoot, H., Barthorpe, S., van der Meer, D., Yang, W.N., Beck, A., Mironenko, T., Hall, C., Hall, J., Mali, I., Richardson, L., Tolley, C., Morris, J., Thomas, F., Lleshi, E., Aben, N., Benes, C.H., Bertotti, A., Trusolino, L., Wessels, L., Garnett, M.J., 2022. Effective drug combinations in breast, colon and pancreatic cancer cells. Nature 603, 166–173.

Jaumot, J., de Juan, A., Tauler, R., 2015. MCR-ALS GUI 2.0: New features and applications. Chemometr. Intell Lab. 140, 1–12.

Karimi, M., Ghasemi, A., Zangabad, P.S., Rahighi, R., Basri, S.M.M., Mirshekari, H., Amiri, M., Pishabad, Z.S., Aslani, A., Bozorgomid, M., Ghosh, D., Beyzavi, A., Vaseghi, A., Aref, A.R., Haghani, L., Bahrami, S., Hamblin, M.R., 2016. Smart micro/nanoparticles in stimulus-responsive drug/gene delivery systems. Chem. Soc. Rev. 45, 1457–1501.

Kaushik, N., Borkar, S.B., Nandanwar, S.K., Panda, P.K., Ha Choi, E., Kaushik, N.K., 2022. Nanocarrier cancer therapeutics with functional stimuli-responsive mechanisms. J. Nanobiotech. 20, 152.

Li, J., Burgess, D.J., 2020. Nanomedicine-based drug delivery towards tumor biological and immunological microenvironment. Acta Pharm. Sin. B 10, 2110–2124.

Li, M.Q., Zhao, G.K., Su, W.K., Shuai, Q., 2020. Enzyme-Responsive Nanoparticles for Anti-tumor Drug delivery. Front. Chem. 8, 647.

Liang, J.G., Yang, B.N., Zhou, X.D., Han, Q., Zou, J., Cheng, L., 2021. Stimuli-responsive drug delivery systems for head and neck cancer therapy. Drug Deliv. 28, 272–284.

Liu, D., Yang, F., Xiong, F., Gu, N., 2016. The Smart Drug delivery System and its Clinical potential. Theranostics 6, 1306–1323.

Liu, B.Y., Wu, W.X., Liu, Y.H., Jia, C., Yang, X.L., Li, J., Wang, N., Yu, X.Q., 2017. Water-soluble mitochondria-targeting polymeric prodrug micelles for fluorescence monitoring and high intracellular anticancer efficiency. Polym. Chem. 8, 5982–5987.

Liu, L., Yang, S.F., Chen, F., Cheng, K.W., 2022. Polysaccharide-Zein Composite Nanoparticles for Enhancing Cellular Uptake and Oral Bioavailability of Curcumin: Characterization, Anti-colorectal Cancer effect, and Pharmacokinetics. Front. Nutr. 9, 846282.

Luo, J.W., Zhang, P., Zhao, T., Jia, M.D., Yin, P., Li, W.H., Zhang, Z.R., Fu, Y., Gong, T., 2019. Golgi Apparatus-Targeted Chondroitin-Modified Nanomicelles Suppress Hepatic Stellate Cell Activation for the Management of Liver Fibrosis. ACS Nano 13, 3910–3923.

Malekjani, N., Jafari, S.M., 2021. Modeling the release of food bioactive ingredients from carriers/nanocarriers by the empirical, semiempirical, and mechanistic models. Compr. Rev. Food Sci. Food Saf. 20, 3–47.

Marsden, H.R., Gabrielli, L., Kros, A., 2010. Rapid preparation of polymersomes by a water addition/solvent evaporation method. Polym. Chem. 1, 1512–1518.

Millard, M., Gallagher, J.D., Olenyuk, B.Z., Neamati, N., 2013. A Selective Mitochondrial-Targeted Chlorambucil with Remarkable Cytotoxicity in Breast and Pancreatic Cancers. J. Med. Chem. 56, 9170–9179.

Prabha, S., Zhou, W.Z., Panyam, J., Labhasetwar, V., 2002. Size-dependency of nanoparticle-mediated gene transfection: studies with fractionated nanoparticles. Int. J. Pharm. 244, 105–115.

Provencher, S.W., 1982. A constrained regularization method for inverting data represented by linear algebraic or integral equations. Comput. Phys. Commun. 27, 213–227.

Qiu, N.S., Gao, J.Q., Liu, Q., Wang, J.Q., Shen, Y.Q., 2018. Enzyme-Responsive Charge-Reversal Polymer-Mediated Effective Gene Therapy for Intraperitoneal Tumors. Biomacromolecules 19, 2308–2319.

Quinn, J.F., Whittaker, M.R., Davis, T.P., 2017. Glutathione responsive polymers and their application in drug delivery systems. Polym. Chem. 8, 97–126.

Shahriari, M., Zahiri, M., Abnous, K., Taghdisi, S.M., Ramezani, M., Alibolandi, M., 2019. Enzyme responsive drug delivery systems in cancer treatment. J. Control. Release 308, 172–189.

Shi, X.Q., Yang, X.Y., Liu, M.Y., Wang, R.J., Qiu, N., Liu, Y.X., Yang, H.T., Ji, J.B., Zhai, G.X., 2021. Chondroitin sulfate-based nanoparticles for enhanced chemo-photodynamic therapy overcoming multidrug resistance and lung metastasis of breast cancer. Carbohydr. Polym. 254, 117459.

Suvarna, M., Dyawanapelly, S., Kansara, B., Dandekar, P., Jain, R., 2018. Understanding the Stability of Nanoparticle-Protein Interactions: effect of Particle size on Adsorption, Conformation and Thermodynamic Properties of Serum Albumin Proteins. Acs Appl. Nano. Mater. 1, 5524–5535.

Tang, L., Yang, X.J., Yin, Q., Cai, K.M., Wang, H., Chaudhury, I., Yao, C., Zhou, Q., Kwon, M., Hartman, J.A., Dobrucki, I.T., Dobrucki, L.W., Borst, L.B., Lezmig, S., Helferich, W.G., Ferguson, A.L., Fan, T.M., Cheng, J.J., 2014. Investigating the optimal size of anticancer nanomedicine. Proc. Natl. Acad. Sci. USA 111, 15344–15349.

Unagolla, J.M., Jayasuriya, A.C., 2018. Drug transport mechanisms and in vitro release kinetics of vancomycin encapsulated chitosan-alginate polyelectrolyte microparticles as a controlled drug delivery system. Eur. J. Pharm. Sci. 114, 199–209.

Wang, X.Y., Li, C., Wang, Y.G., Chen, H.B., Zhang, X.X., Luo, C., Zhou, W.H., Li, L.L., Teng, L.S., Yu, H.J., Wang, J.C., 2022. Smart drug delivery systems for precise cancer therapy. Acta Pharm. Sin. B 12, 4098–4121.

Yi, W., Yan, D., Wang, D., Li, Y., 2023. Smart drug delivery systems to overcome drug resistance in cancer immunotherapy. Cancer Biol. Med. 20, 248–267.

Yu, J.M., Xie, X., Wang, L.L., Liu, W.B., Xu, H.F., Lu, X.M., Li, X.F., Ren, J., Li, W.D., 2023. Smart Chondroitin Sulfate Micelles for Effective Targeted delivery of Doxorubicin against Breast Cancer Metastasis. Int. J. Nanomedicine 18, 663–677.

Zhang, H.B., Zhang, Y.B., Chen, Y.L., Zhang, Y., Wang, Y.G., Zhang, Y.Y., Song, L., Jiang, B.L., Su, G.H., Li, Y., Hou, Z.Q., 2018. Glutathione-responsive self-delivery nanoparticles assembled by curcumin dimer for enhanced intracellular drug delivery. Int. J. Pharm. 549, 230–238.

Zhou, W.X., Jia, Y.J., Liu, Y.N., Chen, Y., Zhao, P.X., 2022. Tumor Microenvironment-based Stimuli-Responsive Nanoparticles for Controlled Release of drugs in Cancer Therapy. Pharmaceutics 14, 2346.